RSC Advances

ROYAL SOCIETY OF CHEMISTRY

www.rsc.org/advances

Table of contents entry

2-Phenyl-3-hydroxy-4-quinolones bind metal ions with selective fluorescence response in aqueous media

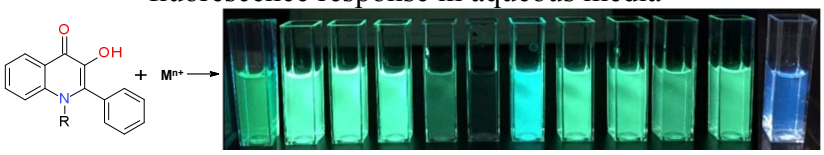

L free **L** Mn^{2+}, Co^{2+},Ni^{2+}, Fe^{3+},Cu^{2+}, Zn^{2+},Cd^{2+}, Hg^{2+}, Pb^{2+}, Eu^{3+}, Me_2Sn^{2+}

Acid-base and coordination properties of 2-phenyl-3-hydroxy-4-quinolones in aqueous media. †

Arturo Jiménez Sánchez and Anatoly K. Yatsimirsky*

Facultad de Química, Universidad Nacional Autónoma de México, 04510 México D.F., México. Fax: 55 5616 2010;Tel: 55 5622 3813; E-mail: anatoli@servidor.unam.mx

† Electronic supplementary information (ESI) available: Electrostatic potential mapped onto total electron density for **1** and **3**, crystallographic data for compound **2**, CCDC 1401533, spectrophotometric and fluorescence titrations of **1** with metal ions. For ESI and crystallographic data in CIF or other electronic formats see DOI:

Table of contents entry

2-Phenyl-3-hydroxy-4-quinolones bind metal ions with selective fluorescence response in aqueous media

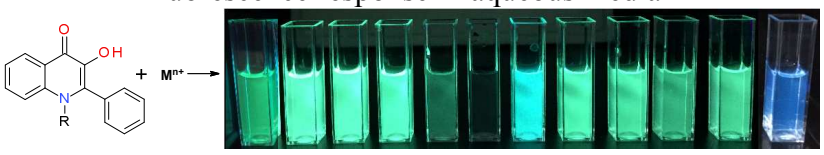

L free **L** Mn^{2+}, Co^{2+},Ni^{2+}, Fe^{3+},Cu^{2+}, Zn^{2+},Cd^{2+}, Hg^{2+}, Pb^{2+}, Eu^{3+}, Me_2Sn^{2+}

Abstract

Acid-base and coordination properties of 2-phenyl-3-hydroxy-4(1*H*)-quinolone (**1**) and 1-methyl-2-phenyl-3-hydroxy-4(1*H*)-quinolone **(2)** were characterized by potentiometric, UV-Visible and fluorescence titrations in water containing 5 or 30% vol. MeCN and in micellar solution of a cationic surfactant. The first dissociation constants (pK_{a1}) corresponding to OH deprotonation of **1** and **2** are about 10 and the ligand **1** undergoes second NH deprotonation with pK_{a2} about 12, which is reduced to 10.4 in the presence of cationic surfactant. More detailed complexation studies were performed with more soluble ligand **1**, which forms stable complexes of 1:1 and 1:2 composition with Fe(III), Cu(II), Zn(II), Pb(II) and Me_2Sn(IV) cations in neutral solutions. The

most unusual behavior is observed with Zn(II), which strongly promotes NH deprotonation of the ligand **1** with formation of the $Zn(L)_2^{2-}$ complex at pH about 8. The formation of this complex is confirmed by results of ^{1}H NMR titrations in DMSO-d_6. Binding of all cations is accompanied by appearance of a new absorption band in the range 385-405 nm with concomitant disappearance of the band at 350-360 nm of the free ligand. Interactions of **1** and **2** with Zn(II) and Me_2Sn(IV) are accompanied by strong and selective fluorescence enhancements with blue shift of the emission bands allowing ratiometric detection of these cations. Complexation with transition and heavy metal ions as well as with lanthanides induces the fluorescence quenching. The ligand **2** is characterized by X-ray crystal structure.

Introduction

Quinolone compounds, both natural and synthetic, possess important biological and medicinal properties including anticancer and antimicrobial activities.[1] A particular group of these compounds constitute 3-hydroxy-4-quinolones, among which 2-heptyl-3-hydroxy-4-quinolone (PQS) serves as a quorum sensing signal molecule[2,3] and 2-phenyl-3-hydroxy-4-quinolones such as **1** and **2** are known to possess anticancer activity, immunosuppressive properties and to act as enzyme inhibitors.[4] 3-Hydroxy-4-quinolones can be considered as aza-analogues of 3-hydoxyflavones. In particular **1** and **2** share common structural features with 3-hydroxyflavone (**3**) and 3-hydroxy-4-pyridinones such as Deferiprone (**4**). The presence of quinolone fragment brings to these compounds interesting fluorescence properties[5] typical for flavones and the presence of 3-hydroxyl group allows the metal ion coordination. The presence of nitrogen atom in **1** and **2** instead of oxygen in **3** should increase the negative charge on carbonyl group and consequently enhance the affinity to metal ions. Indeed reported $\log\beta_1 = 14.6$ for complexation of Fe(III) with 2-methyl-3-hydroxy-4-quinolone [3] is larger than $\log\beta_1 = 13.3$ for complexation with **3**[6] and is approaching that for **4** ($\log\beta_1 = 15.01$)[7], which is one of the most powerful iron(III) chelators. Also calculations of the electrostatic potentials for the ground state of **1** and **3** using DFT at the PBE0/G-31+G(d,p) level of theory (Figure S1, ESI†) predict a significantly increased negative charge on 4-carbonyl group of **1** as compared to **3** with very little change in the electronic density on 3-OH group.

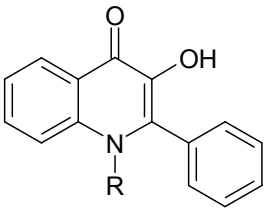

R = H (**1**)
R = Me (**2**)

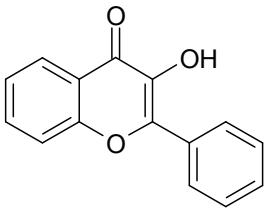

3

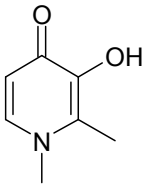

4

Although **3** possesses rather modest metal ion affinity studied mostly in organic solvents [8,9] it finds applications for fluorescence determination of different metal ions such as Al(III) and organotin(IV) compounds [10] and metal complexes of 3-hydroxyflavonoles were tested for their biological activities.[11] Not surpringly metal complexes of 3-hydroxy-4-quinolones, which should be more powerful ligands have attracted significant attention. A study of cytotoxicity as well as DNA binding and cleavage activity of mixed ligand Cu(II) complexes of **1** showed promizing results.[12] Cytotoxic activities of Ru^{II}(arene) complexes of **1** were studied in comparison with related 3-hydroxyflavone complexes.[13] The Zn(II) complex of **1** was prepared and characterized by its cytotoxic activity and spectroscopic properties.[14] Crystal structures of several Cu(II)[15,12] and a Zn(II)[14] complexes of **1** were reported demonstrating expected type of metal ion coordination through deprotonated 3-hydroxyl and 4-carbonyl groups. At the same time no solution studies of complexation of **1** and **2** or their derivatives were reported yet. Such studies are of interest for several reasons. First, the biological activity of 3-hydroxy-4-quinolones is related to their ability to bind intracellular inorganic cations.[16] Second, due to their intense fluorescence they can find applications for sensitive and possibly selective analytical detection of metal ions.[17] Third, the metal complexes of 3-hydroxy-4-quinolones may by themselves serve as optical sensors for anions-(for anion sensing with flavonol complexes see [18,19]).

In this paper we report a detailed study of acid-base and co-ordination properties of **1** and **2** in aqueous media. A very low solubility of both compounds in water represented a serious obstacle for experimental measurements. With more soluble **1** it was possible to obtain reproducible spectrophotometric and fluorescence results with 5% vol. MeCN, although for potentiometric titrations it was necessary to increase the organic co-solvent content to 30% vol. With less soluble **2** results obtained under such conditions were poorly reproducible. We found, however, that both ligands could be studied without problems in the presence of cationic surfactant hexadecyltrimethylammonium bromide (HTAB) at 5 mM concentration, which is well

above its critical micelle concentration. Using of micellar media in this case not only solve the solubility problems, but is of interest by itself because being poorly soluble and highly hydrophobic compounds **1** and **2** and their analogs applied *in vivo* would be most probably bound to cellular membarnes or proteins. In this context it is worth noting that liposomal solubilization of 3-hydroxyquinolones was suggested for their *in vitro* and *in vivo* testing[20] and PQS as well as other related quorum sensing molecules form micelles with very low critical micelle concentrations (9 μM for PQS) in aqueous solutons.[21]

Results and Discussion

Crystal structures of the ligands

The ligand **1** has been characterized by the crystal structure previously.[12] Here we report in addition the crystal structure of **2**, Figure 1. Compound **2** crystallizes in triclinic P-1 space group containing one molecule in the asymmetric unit. A comparison with **1** reveals one significant conformational difference: the torsion angles for the N–C1–C11–C12 fragment in **1** and **2** are 38.96° and 64.22°, respectively. The larger angle in **2** can be attributed to the steric hindrance induced by the N-methyl group. The C1–C2 and C3–O2 distances are significantly smaller in **2** than in **1**, indicating a stronger quinoid character in the former molecule. As expected, the carbonyl and hydroxyl groups constitute a hydrogen bond acceptor and donor moieties in both molecules (Figure 1B). Crystal data and structure refinement for **2** are shown in Table S1 (ESI†).

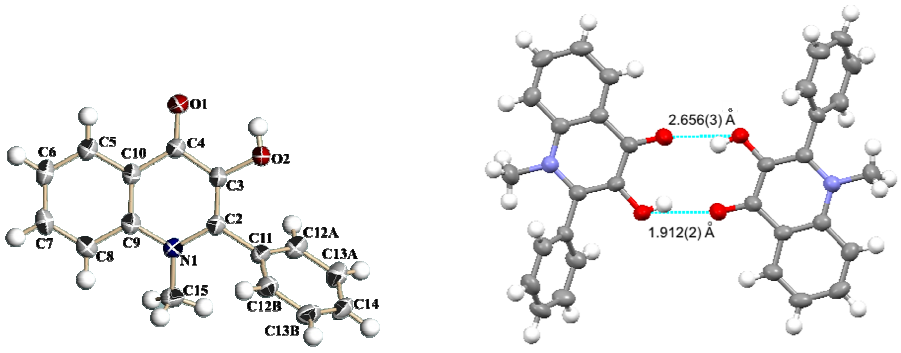

A B

Figure 1. (A) ORTEP diagram for **2**. Ellipsoids are shown at the 50% probability level. (B) Hydrogen bond interactions in **2**.

Acid dissociation constants

Due to solubility problems (see Introduction) the acid dissociation constants of **1** were determined in 5% and in 30% vol. MeCN as well as in 5 mM HTAB while the dissociation constants of **2** were measured only in 5 mM HTAB solution. In the following discussion the medium containing 5% MeCN will be labeled as "aqueous solution" and the medium containing 5 mM HTAB as "micellar solution" for brevity.

Figure 2 shows the absorption spectra of **1** recorded at variable pH. In both media increase in pH induces appearance of a new red shifted absorption band around 400 nm and disappearance of the band at 355-360 nm. In aqueous solution (Figure 2A) these changes occur with preservation of four isosbestic points indicating co-existence of only two forms of the compound, but in micellar solution (Figure 2B) the isosbestic points are not preserved. The absorbances vs. pH profiles at fixed wavelengths shown in inset of the Figure 2B clearly demonstrate at least two deprotonation processes.

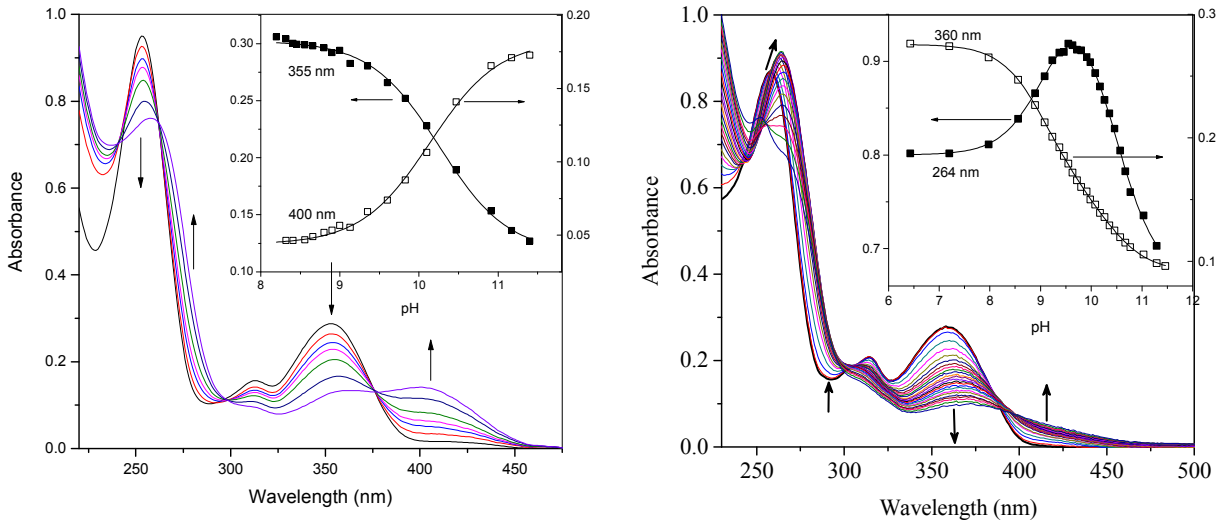

Figure 2. UV-Visible spectra of 40 μM **1** at variable pH (25 °C and 0.05 M NaCl): (A) in 5% MeCN, pH 8.3-11.4; (B) in 5 mM HTAB , pH 6.5-11.5. Insets show absorbance vs. pH profiles at selected wavelengths; solid lines are the theoretical fitting profiles to the equation (1) or (2). Arrows show directions of the spectral changes on increase in pH.

The fitting of the titration results to HypSpec allowed us determination of the respective pK_{a1} and pK_{a2} values given in Table 1.

Table 1. Dissociation constants of **1** and **2** obtained from UV-Vis and fluorescence pH-titrations at 25 ^{o}C and 0.05 M NaCl.

Ligand	**Medium**	**pK_{a1}**		**pK_{a2}**		**Ref**
		UV-Vis	Fl	UV-Vis	Fl	
1	5% MeCN	10.2±0.1	10.8±0.1			this work
1	5 mM HTAB	9.1±0.1	9.15±0.06	10.4±0.1	9.7±0.1	this work
2	5 mM HTAB	9.65±0.08	9.97±0.05			this work
3	50% EtOH/water	9.99				6
3	5 mM HTAC [a)]	6.72				18
4	water	9.82				7

[a)] HTAC is hexadecyltrimethylammonium chloride.

The results of fluorescence pH-titrations of **1** in both media are shown in Figures 3A,B. In aqueous solution two emission bands are observed: one at 494 nm and another one at 412 nm. This type of the emission spectrum was interpreted as a result of excited state intramolecular proton transfer with the band at longer wavelengths belonging to emission from the tautomeric form with proton transferred from 3-OH group to 4-carbonyl group and the band at shorter wavelength belonging to "normal" structure.[5a] In micellar solution the intensity of the emission from the "normal" form strongly decreases. Deprotonation of the ligand quenches the fluorescence and again the titrations profiles correspond to mono-deprotonation in aqueous solution, but double deprotonation in micellar solution clearly seen in the pH-profile of the fluorescence intensity at 470nm (inset in Figure 3B). The respective pK_a values are given in Table 1.

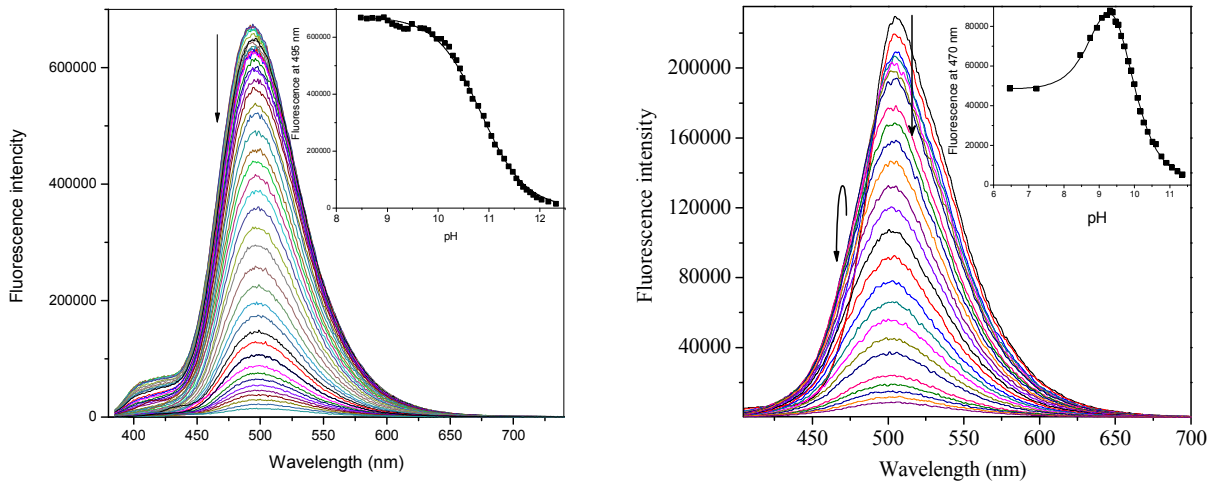

Figure 3. Fluorescence spectra of 40μM **1** at variable pH: (A) in 5% MeCN, (B) in 5 mM HTAB. Insets show fluorescence vs. pH profiles at selected wavelengths. Arrows show directions of the spectral changes on increase in pH. The excitation wavelength is 373 nm (A) and 385 nm (B).

Figure 4 shows spectrophotometric and fluorescence pH-titrations of **2** in micellar solution. The changes in UV-Vis spectra induced by deprotonation of this ligand are similar to those observed with **1**, but fluorescence of **2** shows a more complex trend: the band at 427 nm disappears while the band at 520 nm becomes more intense. This observation agrees with the absence of tautomeric forms in the deprotonated molecule.

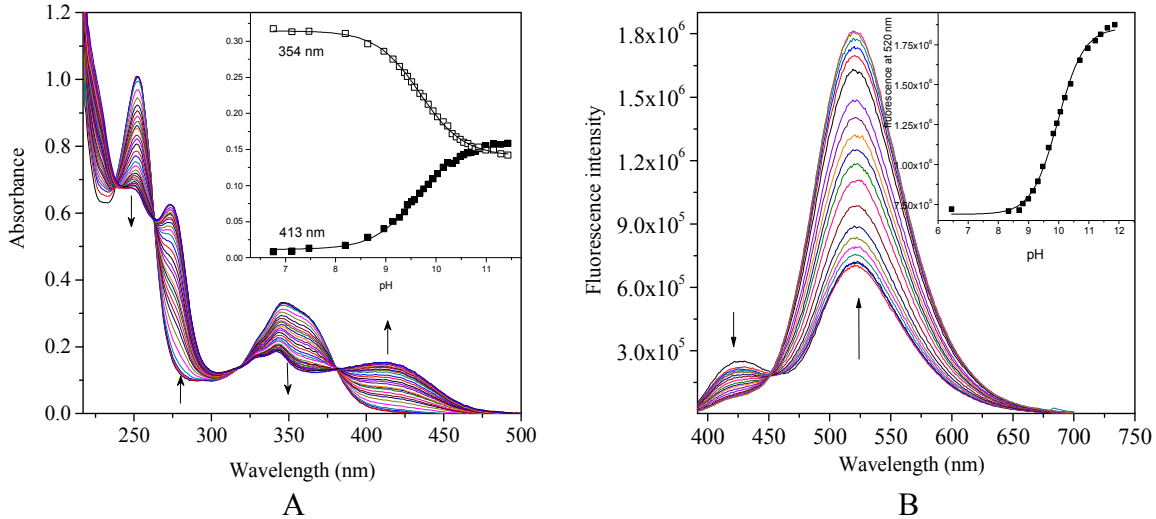

Figure 4. UV-Visible (A) and fluorescence (B) spectra of 40μM **2** at variable pH (6.5-11.5) in 5 mM HTAB. Insets show absorbance or fluorescence vs. pH profiles at selected wavelengths. Arrows show directions of the spectral changes on increase in pH. The excitation wavelength is 385 nm.

The results of all spectroscopic titrations are summarized in Table 1 together with some relevant literature data. Spectrophotometrically determined pK_{a1} of **1** in aqueous solution is close to pK_a values reported for **3** and **4**. A larger value found from fluorescence titration probably involves a contribution from excited state dissociation with shifted pK_a* value. In micellar solution one observes decreased pK_a values due to stabilization of the anionic deprotonated form of **1** by the positive surface charge of the cationic micelle. Similar effect was reported for **3** (see Table 1, lines 4 and 5). Surprisingly we observed a second deprotonation process for **1** in micellar solution, which can be attributed to the deprotonation of N-H group (Scheme 1). Previously the N-deprotonation of 3-hydroxy-2(1H)-pyridinone ligands was observed in their Fe(III) complexes,[22] but for a free ligand this type of dissociation is unusual. However, the quantum chemical calculations using a PBE0/6-31+G(d,p)/IEF-PCM level of theory (two water molecules were included in the model in order to take into account explicit interactions) predicted that NH deprotonation in **1** indeed is quite feasible with calculated pK_{a1} = 9.1 and pK_{a2} = 10.5 close to experimental values obtained in micellar solution.

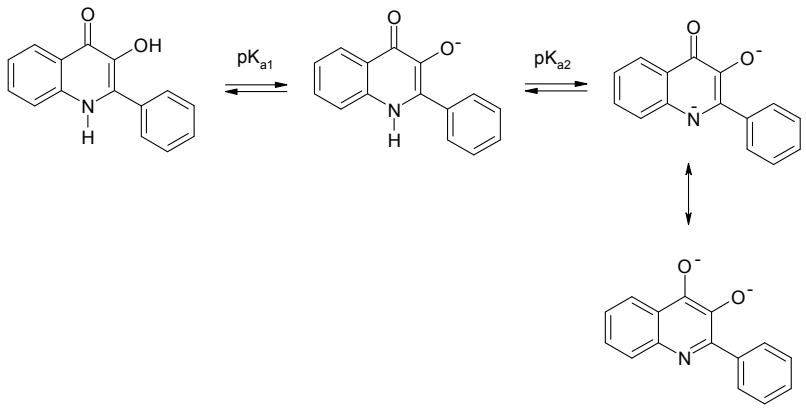

Scheme 1

Metal-ion complexation studies

Interactions of the ligands with metal ions were studied by potentiometric and spectroscopic titrations. With more soluble **1** potentiometric titrations requiring relatively high concentrations of components above 1 mM were performed in 30% vol. MeCN. With **2** the precipitation occurred even in this medium. Titrations in the presence of HTAB, which prevented

precipitation, did not give reproducible results. Therefore with this ligand only spectroscopic titrations in micellar solution employing less than 0.1 mM **2** were performed.

The results of potentiometric titrations were analyzed in terms of traditional *pqr* scheme expressed by equations (1) and (2), where L is a completely deprotonated dianionic form of the ligand and M is the metal ion. The overall binding constants and the appropriate pK_a values of free **1** and complexes are collected in Table 3.

$$pM + qL + rH \rightleftharpoons M_pL_qH_r \quad (1)$$

$$\beta_{pqr} = [M_pL_qH_r]/[M]^p[L]^q[H]^r \quad (2)$$

Table 2. Protonation constants of ligands and stability constants of metal complexes determined potentiometrically in 30% vol. MeCN, 0.05 M NaCl at 25°C.

species	**logβ_{pqr}**	**equilibrium**	**log*K***
LH	11.90±0.01	L + H = LH	11.90
LH_2	22.56±0.01	LH + H = LH_2	10.66
ZnLH	18.94±0.04	Zn + LH = Zn(LH)	7.04
ZnL_2	22.0±0.1	Zn + 2L = $Zn(L)_2$	22.0
CuL_2H_2	46.1±0.1	Cu + 2LH = $Cu(LH)_2$	22.4
CuL_2H	35.4±0.1	$Cu(LH)_2$ = Cu(LH)L + H	-10.7
$SnMe_2LH$	25.12±0.09	$SnMe_2$ + LH = $SnMe_2$(LH)	13.22
$SnMe_2L_2H_2$	45.47±0.08	$SnMe_2$ + 2LH = $SnMe_2(LH)_2$	21.67
		$SnMe_2$(LH) + LH = $SnMe_2(LH)_2$	8.45
$SnMe_2L_2H$	34.7±0.1	$SnMe_2(LH)_2$ = $SnMe_2$(LH)L + H	-10.77

Titration of the free ligand **1** confirms the existence of two deprotonation processes with pK_{a1} = 10.66 close to the value found in 5% MeCN (Table 1) and very high pK_{a2} = 11.9 not detected spectroscopically without surfactant.

In case of Zn(II) two complexes are formed: one of the $M(LH)^+$ composition with mono-deprotonated ligand, which correspond to the reported crystal structure of the isolated Zn(II) complex of **1**,[14] and another one of the ML_2^{2-} composition with doubly deprotonated ligand (see Scheme 2). The first complex is dominating at pH about 7 and the second complex is dominating at pH equal and above 8 (see Figure S2 in ESI† for the calculated species distribution profile).

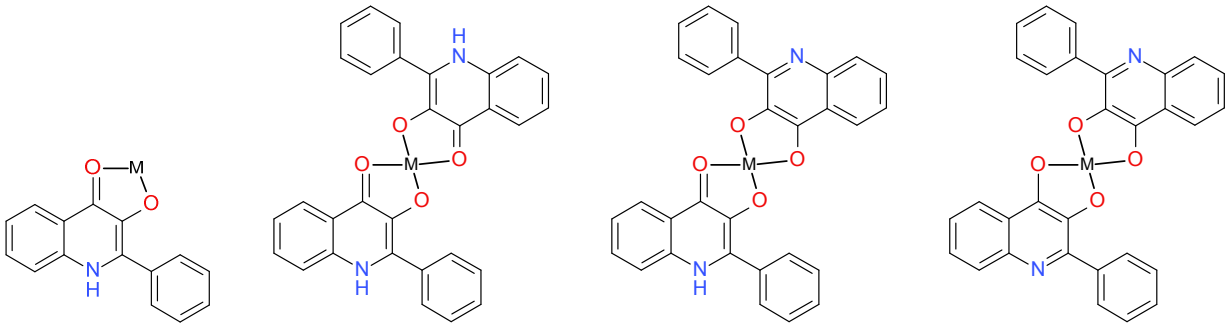

Scheme 2. Types of metal complexes of **1** (LH_2) established by potentiometric titrations

In order to prove formation of the complex with doubly deprotonated ligand interaction of **1** with Zn(II) was followed by ^{1}H NMR in DMSO-d_6. The spectrum of the mixture of **1** with $ZnCl_2$ at molar ratio 2:1 in DMSO (Figure 5A, bottom) coincides with the spectrum of free ligand indicating the absence of interaction. Additions of 0.5 and 1 equivalents of Et_3N respective to **1** to the mixture induce changes in the signals of aromatic protons and a downfield shift with broadening in the signal of NH proton (spectra 2 and 3, Figure 5A). At the same time the signals of Et_3N appear at the positions corresponding to protonated amine (signals of CH_2 and CH_3 groups of free base are observed at 2.41 and 0.93 ppm while corresponding signals of the protonated form at 3.08 and 1.17 ppm respectively). This behavior is consistent with predominant formation of the complex with a mono-deprotonated form of the ligand. When more than 1 equivalent of Et_3N is added the signal of NH proton starts to disappear and the signals of ethyl groups of Et_3N start to move upfield towards positions of the signals of free base, although still remain closer to the signals of the protonated form. Assuming that the observed chemical shifts of methyl and methylene groups of triethylamine are the weighted averages of the signals of free base and protonated forms, as should be in the case of the fast exchange, we calculated the concentration of the protonated form as a function of total triethylamine concentration shown in Figure 5B as a profile of $[Et_3NH^+]$ vs. $[Et_3N]_{Total}$. It demonstrates that formation of Et_3NH^+ reaches the limiting concentration of 20 mM, which is exactly twice the total concentration of **1**. This observation together with disappearance of the NH signal proves the complete deprotonation of the ligand in the presence of Zn(II) at the molar ratio 1:2 and therefore formation of the complex of the ML_2^{2-} type.

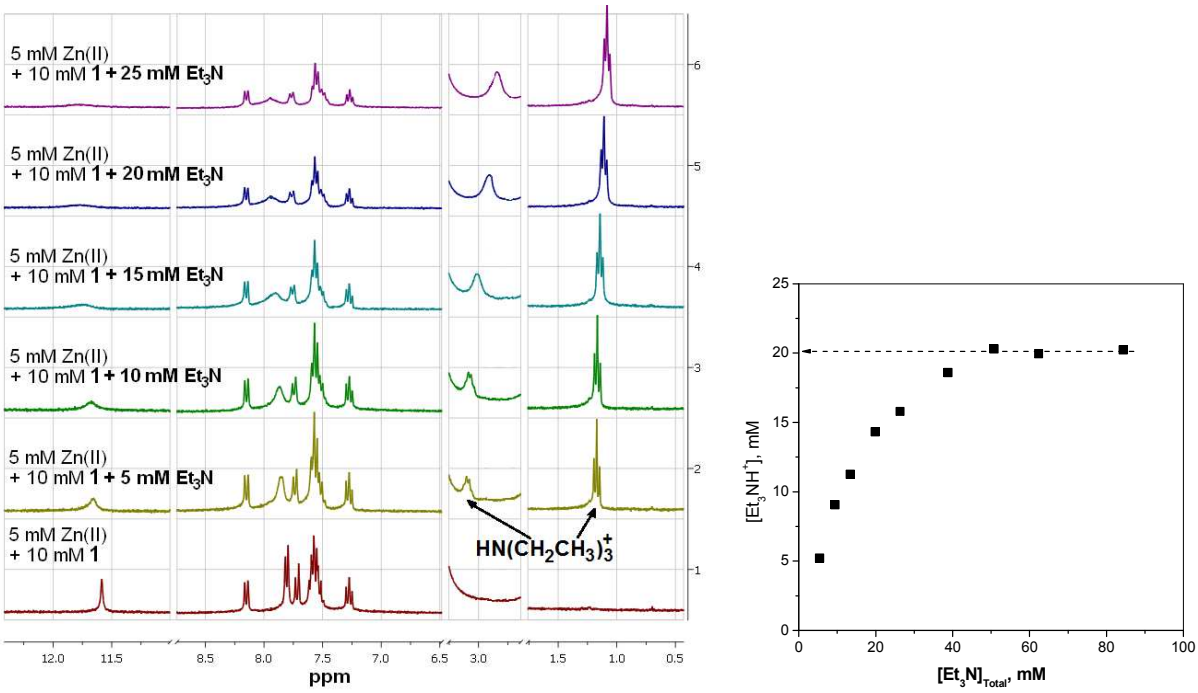

Figure 5. (A) ^{1}H NMR spectra of the mixture of 5 mM $ZnCl_2$ and 10 mM **1** in DMSO-d_6 in the presence of increased amounts of Et_3N. Intervals of chemical shifts containing solvent signals (2.5 ppm for DMSO and 3.3 ppm for traces of water) are eliminated. (B) Concentration of the protonated form of Et_3N as a function of total Et_3N concentration added to a mixture of **1** and Zn(II).

Results for Cu(II) showed that in this case the formation of a 1:1 complex was negligible. The predominant form in neutral solution is a 1:2 complex of the composition $M(LH)_2$ which at high pH is transformed with pK_a = 10.7 into $M(LH)L^-$ containing one mono and one doubly deprotonated ligands. This pK_a is only 1.2 units lower than the pK_{a2} of the free ligand. At the same time formation of the complex ZnL_2^{2-} implies much stronger reduction in pK_{a2} of **1** on coordination to Zn(II). The type of equilibria involved in formation of Zn(II) complexes does not allow one to estimate the pK_{a2} of the coordinated ligand, but the species distribution profile in Figure S2 (ESI†) indicates that it must be below 8. It seems therefore that more electrophilic Cu(II) cation surprisingly is less effective in inducing the second deprotonation of the ligand than Zn(II).

With Me_2Sn^{2+} complexes of three types are observed (Table 2). The simple 1:1 complex of the type $M(LH)^+$ is much more stable with this cation than with Zn(II) and is a dominating species in acid and neutral solutions. With excess of the ligand and pH about and above 7 the $M(LH)_2$ complex is the dominating species, although it has lower stability than the respective

Cu(II) complex (see Table 2). At higher pH this complex is transformed with pK_a = 10.77 into $M(LH)L^-$ species indicating similar effects of $Me_2Sn(IV)$ and Cu(II) on the acidity of NH group.

Spectroscopic, UV-Vis and fluorescence, titrations of **1** were performed with a large set of metals at pH 7 with the purpose to estimate the selectivity of complexation and to evaluate the applicability of **1** for optical sensing of metal ions. The same reaction media, 5% MeCN and 5 mM HTAB were employed as for the spectroscopic pK_a determinations. Although measurements were performed in media different from that employed for potentiometric titrations the complexation stoichiometry should be similar and also there should be at least an approximate agreement between observed stability constants (K_{obs}) experimentally determined from spectroscopic data at a fixed pH value and the values of K_{obs} calculated for a given pH from potentiometric results. As will be shown below such agreement indeed generally is confirmed.

Among tested cations additions of alkaline-earth cations (Mg^{2+} and Ca^{2+}) and Bi(III) did not change neither UV-Vis no fluorescence spectra of **1**. Visual effects of other 11 cations on florescence of **1** at pH 7 are compared in Figure 6. "Naked eye" detectable effects are observed with Fe(III) and Cu(II) inducing the fluorescence quenching and with Zn(II) and $Me_2Sn(IV)$ inducing blue shifts of the emission bands.

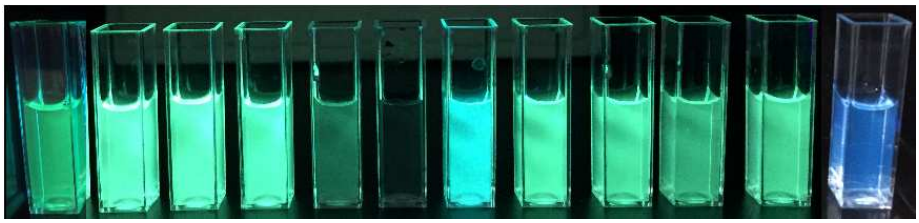

free **1** Mn^{2+}, Co^{2+},Ni^{2+}, Fe^{3+},Cu^{2+}, Zn^{2+},Cd^{2+}, Hg^{2+}, Pb^{2+}, Eu^{3+}, $SnMe_2^{2+}$

Figure 6. Visual effects of metal ions (40 μM) on florescence of 40 μM **1** at pH 7 in 5% MeCN. Excitation at 356 nm.

Figure 7 illustrates titration results with Zn(II) in aqueous solution. Essentially similar results were obtained in micellar solution (Figure S3, ESI†). The fitting of the titration results to HypSpec revealed formation of a 1:1 complexes with the logarithms of the observed stability constants K_{obs} given in Table 3.

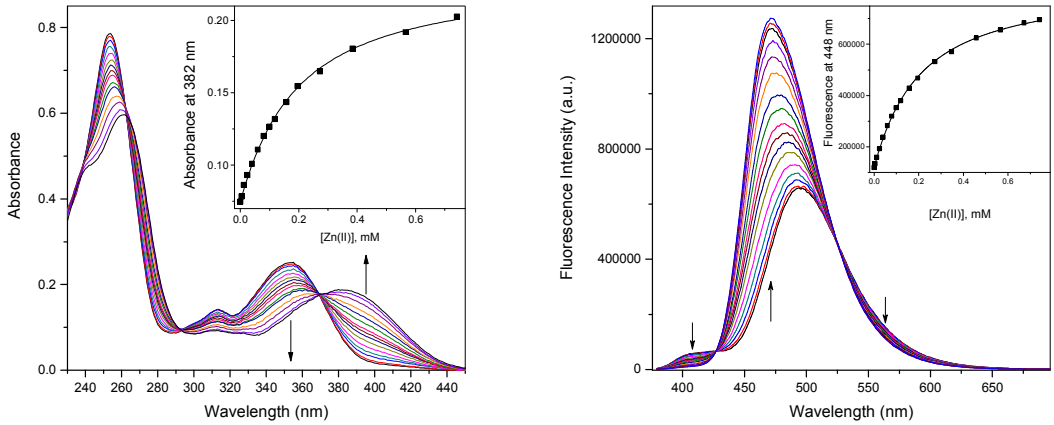

A B

Figure 7. UV-Visible (A) and fluorescence (excitation at 370 nm) (B) spectra of 40 μM **1** in 5% MeCN at pH 7 and variable concentration of Zn(II). Insets show absorbance or fluorescence vs. Zn(II) concentration profiles at selected wavelengths. Arrows show directions of the spectral changes on increase in Zn(II) concentration.

Table 3. Observed stability constants ($logK_{obs}$) and complexation-induced changes in absorption and emission maxima of **1** at pH 7 in 0.05 M NaCl at 25°C. [a)]

Metal ion	5% vol. MeCN					5 mM HTAB				
	$logK_{11}$	$logK_{12}$	λ_{max} Abs [b)]	λ_{max} Fluor	I/I_0 [c)]	$logK_{11}$	$logK_{12}$	λ_{max} Abs [b)]	λ_{max} Fluor	I/I_0 [c)]
None			353	494				359	508	
Mg^{2+}	no interaction									
Ca^{2+}	no interaction									
Mn^{2+}	2.45		400	494	0.920	2.04		406	507	0.942
Fe^{3+}	5.97	9.71	415	quenching	0	6.33	11.83	396	quenching	0
Co^{2+}	3.08		402	495	0.590	3.41		405	506	0.717
Ni^{2+}	3.55		402	494	0.318	3.60		405	506	0.457
Cu^{2+}		12.29	405	quenching	0		13.21	404	quenching	0
Zn^{2+}	3.76		384	471	2.894	3.54		398	472	3.581
Zn^{2+} (pH 8)	4.32		385	472	3.063	4.02	9.61	409	473	3.105
Cd^{2+}	2.73		401	488	1.066	3.02		403	503	1.010
Me_2Sn^{2+}	4.41		422	452	12.316	4.4	9.8	394	452	8.354
Hg^{2+}	< 2		398	494	0.646	< 2		359	507	0.952
Pb^{2+}	5.68	9.62	383	488	0.173	4.39	10.47	384	502	0.065
Eu^{3+}	4.75		390	493	0.130	4.25		386	506	0.097
Bi^{3+}	no interaction									

[a)] Mean values between stability constants determined by spectrophotometric and fluorescence titrations; relative error less or equal to ±0.05.
[b)] The longest wavelength absorption band.
[c)] The ratio of fluorescence intensities at saturation and in the absence of metal ion at the wavelength of the emission maximum of the complex.

Since potentiometric results indicated a change in the stoichiometry at increased pH, titrations were repeated also at pH 8. In aqueous solution only a tighter binding of the same 1:1 stoichiometry was observed, but in micellar solution expected change to predominantly 1:2 metal to ligand complexation was confirmed (Figure 8): the UV-Vis titration plot (Figure 8A, inset) clearly shows the saturation at 1:2 molar ratio and the fluorescence (Figure 8B) initially drops down due to formation of a less fluorescent 1:2 complex and then with excess of the metal ion appears a more intense band at 471 nm characteristic for the 1:1 complex.

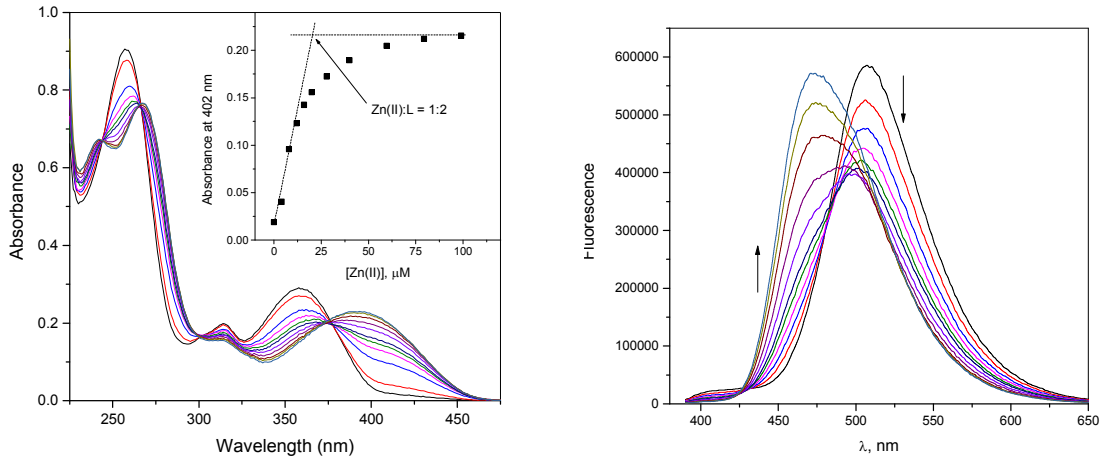

A B

Figure 8. UV-Visible (A) and fluorescence (excitation at 376 nm) (B) spectra of 40 μM **1** in 5 mM HTAB at pH 8 and variable concentration of Zn(II). Insets show absorbance or fluorescence vs. Zn(II) concentration profiles at selected wavelengths. Arrows show directions of the spectral changes on increase in Zn(II) concentration.

In the pH range 7-8 the actual forms of the reactants are Zn^{2+} and LH_2 and the reaction of complex formation for the $M(LH)^+$ species is given by the equation (3).

$$Zn^{2+} + LH_2 = Zn(LH)^+ + H^+ \quad (3)$$

The respective expression for K_{obs} takes the form of the equation (4).

$$\log K_{obs} = \log\beta_{111} - \log\beta_{012} + pH \quad (4)$$

With stability constants given in Table 2 one obtains $\log K_{obs}$ = 3.38 and 4.38 at pH 7.0 and 8.0 respectively, which are reasonably close to the experimental values in both aqueous and micellar solutions given in Table 3.

Similar analysis for formation of the complex ML_2^{2-} predicts that the respective expression for K_{obs} takes the form of the equation (5).

$$\log K_{obs} = \log\beta_{120} - 2\log\beta_{012} + 4pH \quad (5)$$

It follows from the equation (5) that $\log K_{obs}$ = 8.88 and 4.88 at pH 8 and 7 respectively. The experimental K_{obs} at pH 8 in micellar solution is even larger than predicted (Table 3), but at pH 7 the complex is not detected at all. This agrees with extremely sharp pH-dependence of K_{obs} in accordance with equation (5).

Titration results for Cu(II) demonstrated similar to Zn(II) changes in UV-Vis spectra, but complete quenching of the fluorescence in both media (Figure S4, ESI†). Fitting of the concentration profiles confirmed formation of only 1:2 complexes in agreement with results of potentiometric titration. The expression for K_{obs} for formation of expected in this case $M(HL)_2$ complex takes the form of the equation (6), which predicts $\log K_{obs}$ = 14.98 at pH 7.0. Somewhat lower experimental values (Table 3) can be attributed to a difference in solvent composition.

$$\log K_{obs} = \log\beta_{122} - 2\log\beta_{012} + 2pH \qquad (6)$$

Titration results for $Me_2Sn(IV)$ are shown in Figures S5 (ESI†) (aqueous solution) and 9 (micellar solution).

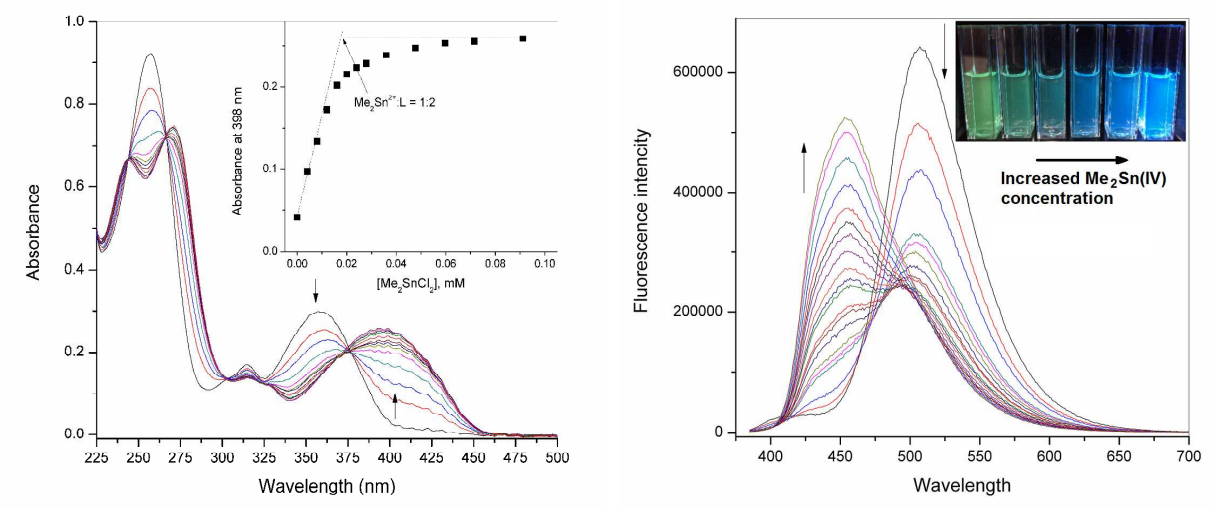

A B

Figure 9. UV-Visible (A) and fluorescence (excitation at 375 nm) (B) spectra of 32 μM **1** in 5 mM HTAB at pH 7 and variable concentration of Me_2SnCl_2. Inset in A shows absorbance vs. Me_2SnCl_2 concentration profile at a fixed wavelength. Inset in B shows visual effects of increased concentrations of Me_2SnCl_2 (0; 0.25; 0.5; 0.75; 1 and 3 equivalents) on the fluorescence of **1**. Arrows show directions of the spectral changes on increase in Me_2SnCl_2 concentration.

The spectral changes observed in the presence of $Me_2Sn(IV)$ resemble those in the presence of Zn(II), but are more pronounced in the fluorescence. This is manifested also in visually much more pronounced blue shift in the fluorescence of **1** in the presence of this cation (see Figure 6). Fitting of the titration results by using the HypSpec revealed formation of 1:1 complexes in aqueous solution, but both 1:1 and 1:2 complexes in micellar solution with K_{obs} collected in Table 3. The pattern of the fluorescence changes in micellar solution resembles that observed with Zn(II) at pH 8 (cf. Figure 8B). The green fluorescence of the free ligand initially disappears due to formation of a less fluorescent 1:2 complex and only with excess of the metal ion one observes appearance of the more intense blue band at 452 nm characteristic for the 1:1 complex (see inset in Figure 9B). Although the stability constant for $Me_2Sn(HL)^+$ complex is 10^6-fold larger than that for $Zn(HL)^+$ (Table 2), the K_{obs} values for these complexes differ less than by one order of magnitude (see Table 3). The reason for this effect is a strong hydrolysis of Me_2Sn^{2+} cation in neutral solutions. In accordance with reported hydrolysis constants in water (pK_{a1} = 3.12, pK_{a2} = 5.33, $\log\beta_{10\text{-}2}$ = -8.45) [23] at pH 7 the cation is completely transformed into dihydroxo complex and the actual reactions of the formation of $M(HL)^+$ and $M(HL)_2$ complexes are (7) and (8) respectively.

$$SnMe_2(OH)_2 + LH_2 + H^+ = SnMe_2(LH)^+ + 2\ H_2O \quad (7)$$

$$SnMe_2(OH)_2 + 2\ LH_2 = SnMe_2(LH)_2 + 2\ H_2O \quad (8)$$

The corresponding values for K_{obs} at pH = 7 are $\log K_{obs} = \log\beta_{111} - \log\beta_{012} - \log\beta_{10\text{-}2} - pH = 4.01$ for $SnMe_2(LH)^+$ and $\log K_{obs} = \log\beta_{122} - 2\log\beta_{012} - \log\beta_{10\text{-}2} = 8.80$ for $SnMe_2(LH)_2$. Comparison with data in Table 3 shows that both calculated K_{obs} are reasonably close to the respective experimental values.

Spectroscopic titrations of **1** with other metal ions are illustrated in Figures S6-S13 (ESI†) and the K_{obs} values together with spectral characteristics of the complexes determined from these results are collected in Table 3. An inspection of the Table 3 reveals the following general features of the complexation processes.

The general stability sequence for divalent transition metal cations follows the Irving-Williams series Mn(II)<Co(II)<Ni(II)<Cu(II)>Zn(II). Very low observed stability for Hg(II) most probably results from its strong hydrolysis and strong binding of this cation to halide anions from the reaction medium. Relatively small K_{obs} for Fe(III), which forms much more stable complex than Cu(II) with ligand **4**,[7] also is a result of strong hydrolysis of Fe(III) in neutral

solution. Relative affinities of cations Cu(II), Zn(II), Cd(II) and Pb(II) are similar to those reported for mimosine and related ligands.[24] The micellar medium affects very little the stability of 1:1 complexes, but promotes formation of 1:2 complexes. This effect can be attributed to increased local concentration of the hydrophobic ligand in the micellar pseudo-phase.[25]

In UV-Vis spectra of **1** the complex formation induces appearance of a new band in the range 385-405 nm with concomitant disappearance of the band at 353 nm (359 nm in micellar solution). Similar spectral change occurs on the deprotonation of the ligand. All metal ions besides Zn(II) and Me_2Sn(IV) induce fluorescence quenching particularly strong with Cu(II) and Fe(III). This is a typical behavior for transition metals. Coordination with Zn(II) induces blue shift and strong enhancement of the fluorescence. The effect of Me_2Sn(IV) depends on the stoichiometry of the complex: formation of a 1:2 complex leads to fluorescence quenching, but 1:1 complex has strong blue fluorescence. Similar behavior was observed previously with diphenyltin(IV) complexes of **3**.[18] The reason of the absence of the fluorescence of the 1:2 complex is not clear yet.

Interactions of metal ions with **2** were studied for comparative purposes with Zn(II), Cu(II) and $SnMe_2$(IV) only in micellar solution. UV-Vis titrations with Zn(II) at pH 7 and 8 (Figure S14, ESI†) indicate formation of 1:1 complexes at both pH with log$K$ = 3.6 and 4.2 respectively. No contribution of a 1:2 complex with this ligand incapable to produce a doubly deprotonated dianionic form is detected at increased pH. Strong 20-fold fluorescence enhancement with a blue shift in the emission maximum is observed, Figure 10A. The fluorescence *vs.* Zn(II) concentration profile fits to the 1:1 complexation equilibrium with the same stability constant as that from UV-Vis results.

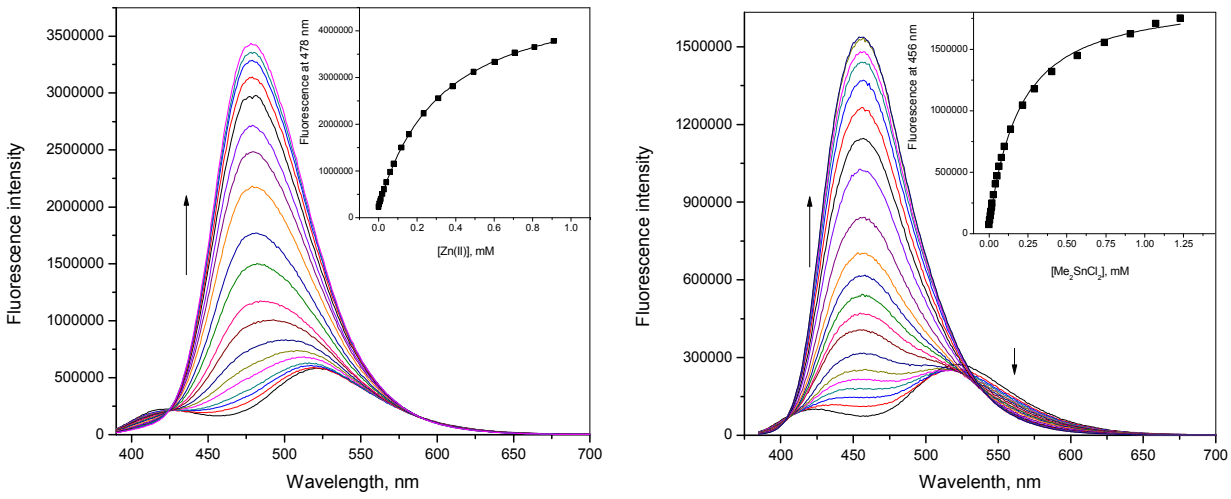

A B

Figure 10. Fluorescence (excitation at 372 nm) spectra of 40 μM **2** in 5 mM HTAB at pH 7 and variable concentration of Zn(II) (A) or Me_2SnCl_2 (B). Insets show fluorescence vs. metal ion concentration profiles at selected wavelengths. Arrows show directions of the spectral changes on increase in metal ion concentration.

Interaction of **2** with Me_2Sn(IV) was accompanied by spectral changes similar to those observed with Zn(II), Figure S14 (ESI†) and 11B. Only a 1:1 complex was formed with $\log K_{11}$ = 4.2 at pH 7.0. Additions of Cu(II) induced a complete quenching of the fluorescence of **2**. Only one complex of the 1:2 stoichiometry was observed with $\log K_{12}$ = 12.7 at pH 7. Thus, towards these two cations, **2** behaves similarly to **1**. An important feature of the results shown in Figure 10 is that together with a strong increase in the fluorescence intensity about 470 nm there are certain wavelengths (425 nm for Zn(II) and 406 nm for Me_2Sn(IV)) where the fluorescence is not changed. This makes possible highly sensitive ratiometric detection of these two cations.

Conclusions

The first dissociation constants of **1** and **2** corresponding to OH deprotonation of 2-phenyl-3-hydroxy-4-quinolones are close to those for 3-hydroxy-flavone and 1,2-dimethyl-3-hydroxy-4-pyridinone, however in contrast to 3-hydroxypyridinones the ligand **1** undergoes second NH deprotonation with pK_a about 12. Comparison of results obtained in water containing 5% vol MeCN and in micellar solution of a cationic surfactant demonstrates certain "micellar effect" manifested in promotion of the second deprotonation of free ligand and preferable formation of

1:2 rather than 1:1 metal complexes. In neutral solutions ligands **1** and **2** have highest affinities to Fe(III), Cu(II) and Pb(II) cations in terms of observed stability constants. The spectral characteristics of the complexation processes demonstrate possible sensitive and selective ratiometric fluorescence detection of Zn(II) and organotin(IV) compounds.

Experimental Section

Materials and physical measurements

Commercially available starting materials, components of buffer solutions (CHES, MOPS, MES) and solvents were used as supplied. Infrared spectra were determined on an FTIR/FIR spectrometer 400 Perkin-Elmer 1600 series. Elemental analyses were carried out on a Perkin-Elmer 2400 CHNS Elemental Analyzer. Melting points were measured on an Electrothermal 9200 apparatus. ^{1}H and ^{13}C NMR spectra were recorded at room temperature on a 300 MHz Varian unity spectrometer. Chemical shifts (ppm) are relative to $(CH_3)_4Si$. Mass spectrometry (MS-FAB+) was obtained by using a Thermo-Electron DFS. Measurements of pH were carried out using an Orion model 710-A research digital pH meter. Fluorescence and UV-Vis absorption spectra were measured on a FluoroMax spectrofluorometer from HORIBA Scientific and Thermo Scientific Evolution diode array UV-Vis spectrophotometer, respectively, equipped with a thermostated cell compartment (recirculating water bath at 25 ± 0.1 °C). Compounds **1** and **2** were synthetized as previously described.[26]

2-Phenyl-3-hydroxy-4(1H)-quinolone (**1**). ^{1}H NMR (300 MHz; DMSO-d_6; Me_4Si): δ 11.64 (br. s, 1H, NH), 8.17 (d, J = 7.8 Hz, 1H, H-5), 7.81 (d, J = 7.1 Hz, 2H, H-12), 7.74 (d, J = 8.4 Hz, 1H, H-8), 7.61–7.52 (m, 4H, H-7, H-13, H-14), 7.28 (t, J = 7.8 Hz, 1H, H-6); ^{13}C NMR (75 MHz; DMSO-d_6; Me_4Si): δ 170.5, 138.5, 138.3, 132.8, 132.1, 131.1, 129.7, 129.7, 128.8, 124.9, 122.5, 122.3 and 118.9. IR (ν_{max}/cm^{-1}) 3197 (O–H stretching), 2922, 2850, 2808 (C–H stretching), 1645 (C=O stretching). Anal. Calc. for $C_{15}H_{11}N_1O_2$ DMF: C 69.66, H 5.85, N 9.03; found: C 69.71, H 5.23, N 9.34. MS (FAB, *m/z*) 237 $[M]^+$; m.p. 276–279 °C.

1-methyl-2-phenyl-3-hydroxy-4(1H)-quinolone (2). ^{1}H NMR (300 MHz; DMSO-d6; Me_4Si): δ 8.15 (d, J = 8.5 Hz, 2H, ArH), 7.81 (d, J = 7 Hz, 2H, Ar'H), 7.72 (d, J = 8 Hz, 1H, ArH), 7.57 (m, 4H, ArH, Ar'H), 7.27 (t, J = 7 Hz, 1H, Ar'H), 355 (s, 3H, N-CH_3); ^{13}C NMR (75 MHz; DMSO-d_6; Me_4Si): δ 169.7, 139.4, 139.3, 137.3, 132.8, 131.7, 130.3, 129.5, 129.0, 125.6, 123.65, 122.6, 117.5 and 37.5. IR (ν_{max}/cm^{-1}) 3387 (O–H stretching), 2925, 2862, 2811 (C–H stretching), 1693 (C=O stretching). Anal. Calc. for $C_{16}H_{13}N_1O_2$: C 76.48, H 5.21, N 5.57; found: C 74.24, H 6.65, N 5.10. MS (FAB, *m/z*) 251 $[M]^+$; m.p. 273–276 °C.

Spectrophotometric and Fluorometric Titrations

All titration experiments were performed at 25 °C and ionic strength 0.05 M created either by buffer or NaCl. The experiments were performed either with 5% vol. MeCN or with 5 mM hexadecyltrimethylammonium bromide (HTAB). An aliquot of 1 mM stock solution of **1** or **2** in acetonitrile was added to a 5 or 50 mM MOPS, MES or CHES aqueous buffered solution in appropriate pH intervals, allowing equilibration for 15 minutes before titrations. The final content of acetonitrile was less than 1% when HTAB was used. The program HypSpec version 1.1.33 was used to calculate all equilibrium constants.

Potentiometric titrations

Potentiometric titrations were performed in a 10-mL thermostatted cell kept under nitrogen at 25 ± 0.1 °C with 0.05 M NaCl as background electrolyte in 30% vol. MeCN with 3 mM **1** and molar ratio metal:ligand = 1:2. Experimental details and procedure for the electrode calibration were the same as in ref. 27 for potentiometric titrations in aqueous DMSO. The autoprotolysis constant of water pK_w = 14.6±0.1 was determined in 30% MeCN in agreement with reported value in this medium.[28] The program Hyperquad 2008[29] was used to calculate all equilibrium constants.

X-ray crystallography

Crystals of **2** were grown by slow evaporation from a saturated DMSO solution of **2** at room temperature. Single-crystals of **2** were studied with Oxford Diffraction Gemini "A"

diffractometer with a CCD area detector ($\lambda_{MoK\alpha}$ = 0.71073 Å, graphite monochromator, T = 293 K) source equipped with a sealed tube X-ray source. Unit cell constants were determined with a set of 15/3 narrow frame/runs (1° in ω) scans. Structure solution and refinement were performed with SHELX-2013 software,[30] and Mercury Crystal Structure Visualization software was used for molecular visualization.[31] WinGX environment program set [32] was used to prepare material for publication. Full-matrix least squares refinement was carried out by minimizing $(Fo^2 - Fc^2)^2$. All non-hydrogen atoms were refined anisotropically. H atom attached to the oxygen atoms was located in a difference map. H atoms attached to C atoms were placed in geometrically idealized positions and refined as riding on their parent atoms, with C − H = 0.98−0.99 Å and U_{iso} (H) = 1.2 U_{eq} (C) for methyl group.

Computational methods

Quantum chemical calculations were obtained by using DFT and TD-DFT with Polarizable Continuum Model [33] as performed in the Gaussian 09 code,[34] using a PBE0/6-31+G(d,p)/IEF-PCM (water) level of theory to determine the optimized molecular geometry of **1** and **3**. Then, a frequency analysis corroborates that this geometry corresponds to an energy minimum, finding no imaginary frequencies. Zero point vibrational energies (ZPVE) were considered to account for thermal and entropic effects during pK_a calculations. As a first step in the analysis of the electron charge distribution in the molecules, the electrostatic potentials were computed to compare the local charge distribution in these molecules. To compute the pK_a values of **1** we use the Born-Haber method.[35] In order to determine the ΔG_{solv} the water solvent was modeled by an implicit (IEF-PCM)–explicit solvent model (IE). In the IE approach two water molecules were included in order to model explicit interactions and its positions were fully optimized as well.

Acknowledgements

Arturo Jiménez Sánchez thanks DGAPA-UNAM for the postdoctoral fellowship.

References

[1] S. Heeb, M. P. Fletcher, S. R. Chhabra, S. P. Diggle, P. Williams and M. Cámara, *FEMS Microbiol. Rev*., 2011, **35**, 247–274.

[2] P. Williams, *Microbiology*, 2007, **153**, 3923–3938.

[3] S. P. Diggle, S. Matthijs, V. J. Wright, M. P. Fletcher, S. Ram Chhabra, I. L. Lamont, X Kong, R. C. Hider, P. Cornelis, M. Cámara and P. Williams, *Chemistry & Biology,* 2007, **14**, 87–96.

[4] P. Hradil, J. Hlavac, M. Soural, M. Hajduch, M. Kolar and R. Vecerova, *Mini Rev. Med. Chem.*, 2009, **9**, 696–702.

[5] (a) D. A. Yushchenko, V. V. Shvadchak, A. S. Klymchenko, G. Duportail, Y. Mély and V. G. Pivovarenko, *New J. Chem.*, 2006, **30**, 774–781; (b) M. D. Bilokin', V. V. Shvadchak, D. A. Yushchenko, G. Duportail, Y. Mély and V. G. Pivovarenko, *J. Fluoresc.,* 2009, **19**, 545–553.

[6] M. D. Engelmann, R. Hutcheson and I. F. Cheng, *J. Agric. Food Chem.,* 2005, **53**, 2953–2960.

[7] V. M. Nurchi, G. Crisponi, T. Pivetta, M. Donatoni and M. Remelli, *J. Inorg. Biochem.*, 2008, **102**, 684–692.

[8] M. M. Kasprzak, A. Erxleben and J. Ochocki, *RSC Advances*, 2015, DOI: 10.1039/C5RA05069C

[9] (a) J. V. Valente, M. A. Buntine, S. F. Lincoln and A. D. Ward, *Inorg. Chim. Acta*, 2007, **360**, 3380–3386; (b) Y. A. Davila, M. I. Sancho, M. C. Almandoz and S. E. Blanco, *Spectrochim. Acta A*, 2012, **95**, 1–7; (c) J. P. Cornard, L. Dangleterre and C. Lapouge, *Chem. Phys. Lett.*, 2006, **419**, 304–308.

[10] (a) M. Katyal and S. Prakash, *Talanta*, 1977, **24**, 367–375; (b) Y. Arakawa, O. Wada and M. Manabe, *Anal. Chem.*, 1983, **55**, 1901–1904; (c) E. González-Toledo, R. Compañó, M. Granados and M. D. Prat, *TrAC Trends Anal. Chem.,* 2003, **22**, 26–33.

[11] (a) K. Grubel, A. R. Marts, S. M. Greer, D. L. Tierney, C. J. Allpress, S. N. Anderson, B. J. Laughlin, R. C. Smith, A. M. Arif, L. M. Berreau and M. Lisa, *Eur. J. Inorg. Chem.*, 2012, **2012**, 4750–4757; (b) K. Grubel, B. J. Laughlin, T. R. Maltais, R. C. Smith, A. M. Arif, L. M. Berreau and M. Lisa, *Chem. Commun.*, 2011, **47**, 10431–10433; (c) M. Grazul and E. Budzisz, *Coord. Chem. Rev.,* 2009, **253**, 2588–2598.

[12] R. Buchtık, Z. Travnıcek, J. Vanco, R. Herchela and Z. Dvorak, *Dalton Trans.*, 2011, **40**, 9404–9412.

[13] A. Kurzwernhart, W. Kandioller, É. A. Enyedy, M. Novak, M. A. Jakupec, B. K. Kepplera and C. G. Hartinger, *Dalton Trans.*, 2013, **42**, 6193–6202.

[14] R. Buchtik, I. Nemec and Z. Trávníček, *J. Molec. Struct.*, 2014, **1060**, 42–48.

[15] M. Czaun, G. Speier and L. Párkányic, *Chem. Commun.,* 2004, 1004–1005.

[16] J. W. Schertzer, M. L. Boulette and M. Whiteley, *Trends Microbiol.*, 2009, **17**, 189–195.

[17] For recent reviews on optical detection of metal ions see: (a) J. Yin, Y. Hu and J. Yoon, *Chem. Soc. Rev*., 2015, Advance Article, DOI: 10.1039/C4CS00275J; (b) G. R. C. Hamilton, S. K. Sahoo, S. Kamila, N. Singh, N. Kaur, B. W. Hyland and J. F. Callan, *Chem. Soc. Rev*., 2015, **44**, 4415-4432; (c) L. Zhu, A. H. Younes, Z. Yuan and R. J. Clark, *J. Photochem. Photobiol. A: Chemistry*, 2015, **311**, 1-15; (d) D. Kim, H. G. Ryu and K. H. Ahn, *Org. Biomol. Chem*., 2014, **12**, 4550-4566; (e) L. Zhu, Z. Yuan, J. Simmons and K. Sreenath, *RSC Adv.*, 2014, **4**, 20398-20440.

[18] R. Villamil-Ramos, V. Barba and A. K. Yatsimirsky, *Analyst*, 2012, **137**, 5229–5236.

[19] Y. Takahashi, D. A. P. Tanaka, H. Matsunaga and T. M. Suzuki, *J. Chem. Soc., Perkin Trans. 2*, 2002, 759–762.

[20] M. Di Cagno, J. Styskala, J. Hlavac, M. Brandt, A. Bauer-Brandt and N. Skalko-Basnet, J. *Liposome Res.*, 2001, **21**, 272–278.

[21] B. M. Davis, J. L. Richens and P. O'Shea, *Biophys. J.*, 2011, **101**, 245–254.

[22] R. C. Scarrow and K. N. Raymond, *Inorg. Chem.,* 1988, **27**, 4140–4149.

[23] A. Casale, C. De Stefano, G. Manfredi, D. Milea and S. Sammartano, *Bioinorg. Chem. Appl.*, 2009, **2009**, Article ID 219818, 17 pages, doi:10.1155/2009/219818.

[24] H. Stunzi, D. Perrin, T. Teitei and R. L. N. Harris, *Aust. J. Chem*., 1979, **32**, 21–30.

[25] I. V. Berezin, K. Martinek and A. K. Yatsimirsky, *Russ. Chem. Rev. (Engl. Transl.)*, 1973, **42**, 787–802.

[26] P. Hradil, J. Hlaváč and K. Lemr, *J. Heterocyclic Chem.,* 1999, **36**, 141–144.

[27] I. Sánchez-Lombardo and A. K. Yatsimirsky, *Inorg. Chem*., 2008, **47**, 2514–2525.

[28] E. Bosch, G. Fonrodona, C. Rafols and M. Roses, *Anal. Chim. Acta,* 1997, **349**, 367–376.

[29] (a) P. Gans, A. Sabatini, A. Vacca, *Talanta,* 1996, **43**, 1739–1753. (b) L. Alderlghi, P. Gans, A. Ienco, D. Peters, A. Sabatini and A. Vacca, *Coord. Chem. Rev.,* 1999, **184**, 311–318.

[30] G. M. Sheldrick, SHEXL-2013; University of Göttingen: Germany, 2013.

[31] C. F. Macrae, I. J. Bruno, J. A. Chisholm, P. R. Edgington, P. McCabe, E. Pidcock, L. Rodriguez-Monge, R. Taylor, J. van de Streek and P. A. Wood, *J. Appl. Crystallogr.,* 2008, **41**, 466–470.

[32] L. J. Farrugia, *J. Appl. Crystallogr.*, 1999, **32**, 837–838.

[33] (a) C. Amovilli, V. Barone, R. Cammi, E. Cancès, M. Cossi, B. Mennucci, C. S. Pomelli and J. Tomasi, *Adv. Quant. Chem.*, 1998, **32**, 227–261; (b) J. Tomasi, B. Mennucci, R. Cammi, *Chem. Rev.* 2005, **105**, 2999–3094.

[34] Gaussian 09, Revision D.01, M. J. Frisch, G. W. Trucks, H. B. Schlegel, G. E. Scuseria, M. A. Robb, J. R. Cheeseman, G. Scalmani, V. Barone, B. Mennucci, G. A. Petersson, H. Nakatsuji, M. Caricato, X. Li, H. P. Hratchian, A. F. Izmaylov, J. Bloino, G. Zheng, J. L. Sonnenberg, M. Hada, M. Ehara, K. Toyota, R. Fukuda, J. Hasegawa, M. Ishida, T. Nakajima, Y. Honda, O. Kitao, H. Nakai, T. Vreven, J. A. Montgomery, Jr., J. E. Peralta, F. Ogliaro, M. Bearpark, J. J. Heyd, E. Brothers, K. N. Kudin, V. N. Staroverov, R. Kobayashi, J. Normand, K. Raghavachari, A. Rendell, J. C. Burant, S. S. Iyengar, J. Tomasi, M. Cossi, N. Rega, J. M. Millam, M. Klene, J. E. Knox, J. B. Cross, V. Bakken, C. Adamo, J. Jaramillo, R. Gomperts, R. E. Stratmann, O. Yazyev, A. J. Austin, R. Cammi, C. Pomelli, J. W. Ochterski, R. L. Martin, K. Morokuma, V. G. Zakrzewski, G. A. Voth, P. Salvador, J. J. Dannenberg, S. Dapprich, A. D. Daniels, Ö. Farkas, J. B. Foresman, J. V. Ortiz, J. Cioslowski, and D. J. Fox, *Gaussian, Inc.*, Wallingford CT, 2009.

[35] (a) Y. Houari, D. Jacquemin and A. D. Laurent, *Phys. Chem. Chem. Phys.,* 2013, **15**, 11875–11882. (b) C. P. Kelly, C. J. Cramer and D. G. Truhlar, *J. Phys. Chem. A* 2006, **110**, 2493–2499.